Slow Dielectric Relaxation of Entangled Linear *cis*-Polyisoprenes with Asymmetrically Inverted Dipoles. 1. Bulk Systems

Hiroshi Watanabe,* Osamu Urakawa, and Tadao Kotaka

Department of Macromolecular Science, Faculty of Science, Osaka University, Toyonaka, Osaka 560, Japan

Received May 3, 1993

ABSTRACT: Global motion of entangled linear *cis*-polyisoprene (PI) chains in monodisperse systems was examined through their slow dielectric relaxation behavior. For this purpose, a series of *dipole-inverted* PI chains of (almost) the *same* molecular weight $M \simeq 48 \times 10^3$ was made *via* multistep coupling of two living PI anion precursors of various M_1 and $M_2 = M - M_1$ ($\leq M_1$) with a bifunctional terminator, *p*-xylylene dichloride. Those PI chains had dipoles that were parallel along the chain contour but inverted once at a contour distance M_2 from one chain end, and their slow dielectric relaxation corresponded to fluctuation of a vector $\Delta\mathbf{R}(t) = \mathbf{R}_1(t) - \mathbf{R}_2(t)$, with $\mathbf{R}_1(t)$ and $\mathbf{R}_2(t)$ being the vectors that connect the dipole inversion (DI) point and the two chain ends at time t. Because of the differences in the DI point locations M_2, the PI chains of (almost) the same M and thus of the same global motion exhibited remarkably different dielectric loss (ϵ'') curves: For PI's with $M_2 = M/2$ (DI at the chain center) and $M_2 = 0$ (DI at chain end, i.e., without DI), the dielectric relaxation time was found to be 3.9 times shorter for the former but the relaxation mode distribution was the same. For $0 < M_2 < M/2$, the ϵ'' curves were intermediate of these two extremes and exhibited a bimodal relaxation mode distribution. These features of the dipole-inverted PI's at low frequencies were reasonably well described by a model considering reptation and Rouse-type constraint release (CR) for the cases of $M_2 = 0$ and $M/2$. However, nonnegligible disagreements were found for the cases of intermediate M_2, indicating a necessity of refining the model. Further analyses of the ϵ'' data enabled us to obtain information on low-order eigenfunctions $f_p(n)$ for a local correlation function $C(n,t;m) = (1/a^2)\langle \mathbf{u}(n,t)\cdot\mathbf{u}(m,0)\rangle$, with $\mathbf{u}(n,t)$ being a bond vector for nth segment at time t and $a^2 = \langle \mathbf{u}^2 \rangle$. The experimental $f_p(n)$ ($p = 1$–3) were not largely but certainly different from the model eigenfunctions and exhibited nonsinusoidal n dependence. This n dependence appeared to be related to an extra relaxation mechanism (other than reptation and Rouse-type CR) that had a significant effect at chain ends.

I. Introduction

Entanglement of long and flexible chains is one of the most fundamental subjects in polymer physics, and some characteristic features like the $M^{3.4-3.7}$ dependence of viscosity of linear chains have been well-known.[1,2] However, details for molecular motion and relaxation processes of entangled chains are not yet completely understood. For investigation of such details, it is most efficient to use some labeling techniques and examine various dynamic quantities for a particular segment and/or chain involved in the system. In this sense isotope labeling has been successfully used, for example, in diffusion and orientation relaxation experiments to elucidate some detailed aspects of the chain motion.[3–5] However, even with such labeling techniques any single experiment can provide us only limited information: The diffusion experiments elucidate only the center-of-mass displacement, while the orientation and viscoelastic relaxation experiments provide information only for anisotropy of chain orientation at *respective* times.[6] For a deeper understanding of the entanglement dynamics, it is desirable to combine all aspects of molecular motion obtained from various kinds of experiments with adequate labeling techniques.

From the above point of view, it is important to examine dielectric relaxation of so-called type-A chains[7] that have dipoles parallel along the chain contour. As pioneered by Stockmayer and co-workers[7,8] and later studied extensively by Adachi and co-workers,[9–11] Boese and co-workers,[12] and Patel and Takahashi,[13] global motion of type-A chains (like poly(propene oxide) and *cis*-polyisoprene chains) induces M-dependent dielectric relaxation processes. These processes provide us information for a correlation of chain orientation at two *separate* times[6,14,15] that is different in nature from the information extracted from the diffusion and orientation as well as viscoelastic relaxation processes explained above. In addition, *dielectric labeling* can be attained for a special sort of type-A chains that have the parallel dipoles inverted once at a particular point in the chain contour[10,14,15] (cf. Figure 1). The dielectric relaxation process of those chains reflects fluctuation of a vector $\Delta\mathbf{R} = \mathbf{R}_1 - \mathbf{R}_2$, with $\mathbf{R}_1$ and $\mathbf{R}_2$ being the vectors that connect the dipole-inversion point and the two chain ends. Namely, the chains having differently located dipole-inversion points should exhibit different relaxation processes even if the molecular motion itself is the same. In this sense, the dipole-inversion works as the dielectric labeling.

On the basis of the above ideas, we have anionically synthesized a unique series of linear *cis*-polyisoprene (PI) chains having almost the same M but dipole inversion at different locations and examined their dielectric relaxation processes. Specifically, analyses for these processes enabled us to obtain entirely new and interesting information on eigenfunctions for a local correlation function that describes an orientation correlation of segmental bond vectors at two separate times.[14,15] This paper explains the method of synthesis for the dipole-inverted PI chains of narrow molecular weight distribution, the dielectric data for their bulk systems, and the resulting information for the eigenfunctions. Results of studies on blends containing the dipole-inverted chains will be described in our later paper.

Here, we emphasize that the dipole-inverted PI chains are the best model chains for investigating the details of the local correlation function. Such details could be examined, *in principle*, also for entangled block polymers like polybutadiene (PB)–PI diblock polymers that are composed of non-type-A (PB) and type-A (PI) blocks.[11] However, even for the chemically similar PB and PI blocks, the entanglement spacing (M_e) and segmental friction (ζ) are considerably different.[14] Thus, such block polymers

0024-9297/93/2226-5073$04.00/0

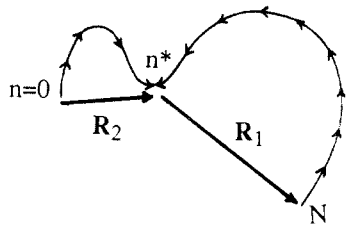

Figure 1. Schematic representation of a PI chain having asymmetrically inverted dipoles.

have a distribution of M_e and ζ along the chain contour, and their modes of molecular motion should be considerably different from the modes for homopolymers. Because of this difference, the dielectric information obtained for the block polymers cannot be used for quantitative discussion on the motion of homopolymers. On the other hand, this problem due to the M_e and ζ distribution never appears for the dipole-inverted *homo*-PI chains, and thus these chains are ideal for the present study.

II. Theoretical Section

We here consider a linear Gaussian chain that is composed of N segments and has the parallel dipoles inverted once at the n^*th segment (cf. Figure 1). We can extract some detailed information for the motion of this chain from its dielectric data, as explained below.

The total polarization of the dipole-inverted chain at a time t is proportional to a vector $\Delta\mathbf{R}(t) = \mathbf{R}_1(t) - \mathbf{R}_2(t)$, with $\mathbf{R}_1(t)$ and $\mathbf{R}_2(t)$ being the vectors connecting the n^*th segment and the two chain ends (cf. Figure 1). Thus, its dielectric relaxation function $\Phi(t)$ normalized to unity at $t = 0$ is written in terms of $\Delta\mathbf{R}$ and the end-to-end vector $\mathbf{R}_e$ as[10,14,15]

$$\Phi(t) = \frac{\langle \Delta\mathbf{R}(t)\cdot\Delta\mathbf{R}(0)\rangle}{\langle \mathbf{R}_e^2\rangle} \tag{1}$$

(Here, we have used a relation $\langle \Delta\mathbf{R}^2\rangle = \langle \mathbf{R}_e^2\rangle$ valid for a Gaussian chain.) The dielectric loss factor ϵ'' is written in terms of Φ as[16]

$$\epsilon''(\omega) = -\Delta\epsilon \int_0^\infty \frac{d\Phi(t)}{dt} \sin \omega t \, dt \tag{2}$$

Here, ω and $\Delta\epsilon$ are the angular frequency and the dielectric relaxation intensity, respectively.

As can be seen from eqs 1 and 2, the slow dielectric relaxation of the dipole-inverted chain reflects fluctuation of the difference vector $\Delta\mathbf{R}$ that is induced by the global chain motion. As a quantity that describes the fundamental aspects of this relaxation, we here introduce a local correlation function[6,14,15]

$$C(n,t;m) = (1/a^2)\langle \mathbf{u}(n,t)\cdot\mathbf{u}(m,0)\rangle \tag{3}$$

with $\mathbf{u}(n,t)$ being a bond vector for the nth segment at time t and $a^2 = \langle \mathbf{u}^2\rangle$ (the mean-square segment size). This function represents an orientation correlation of the nth and mth bond vectors at two separate times, so that it contains detailed information for the global chain motion. Assuming a very rapid orientation randomization for two bond vectors at the chain ends, we have a boundary condition for C,

$$C(n,t;m) = 0 \qquad \text{for } n, m = 0, N \tag{4}$$

For a Gaussian chain having no isochronal orientation correlation for different bond vectors, we may write the initial condition as[14,15,17]

$$C(n,0;m) = \delta_{nm} = \frac{2}{N}\sum_{p=1}^{N} \sin\frac{p\pi n}{N} \sin\frac{p\pi m}{N} \tag{5}$$

From eqs 1 and 3, the relaxation function Φ is related to the local correlation function as

$$\Phi(t;n^*) = \frac{1}{N}[\int_0^{n^*} dn - \int_{n^*}^{N} dn][\int_0^{n^*} dm - \int_{n^*}^{N} dm]C(n,t;m) \tag{6}$$

This relation clearly indicates that Φ and thus ϵ'' (cf. eq 2) change with n^* even if the molecular motion described by $C(n,t;m)$ is the same. In other words, using eq 6 to analyze the n^*-dependent ϵ'' data of the dipole-inverted PI chains, we can find features of $C(n,t;m)$, i.e., how the orientation correlation of two particular bond vectors changes with time. (Note again that the dipole inversion works as dielectric labeling to provide this information.)

For convenience of the above analysis, we expand $C(n,t;m)$ at long time scales with respect to its *eigenfunctions* $f_p(n)$ (with the mode number $p = 1, 2, \ldots, N$). The functional form of $f_p(n)$ is determined by a time evolution equation for $C(n,t;m)$, i.e., by a nature of the global chain motion. As discussed in Appendix A, we may use f_p and generally write $C(n,t;m)$ in the form

$$C(n,t;m) = \frac{2}{N}\sum_{p=1}^{N} f_p(n)\, f_p(m) \exp(-t/\tau_p) \tag{7}$$

Here, τ_p is the pth relaxation time (=reciprocal of the pth eigenvalue). The f_p's involved in eq 7 satisfy a boundary condition (cf. eq 4)

$$f_p(0) = f_p(N) = 0 \tag{8}$$

and a normalization condition (cf. eq 5)

$$\frac{2}{N}\sum_{p=1}^{N} f_p(n)\, f_p(m) = \delta_{nm} \tag{9}$$

From eqs 1, 2, 6, and 7, we find

$$\epsilon''(\omega;n^*) = \sum_{p=1}^{N} g_p(n^*) \frac{\omega\tau_p}{1+\omega^2\tau_p^2} \tag{10}$$

Here, g_p is the intensity of the pth dielectric mode,

$$g_p(n^*) = \frac{2\Delta\epsilon}{N^2}[\int_0^{n^*} f_p(n)\, dn - \int_{n^*}^{N} f_p(n)\, dn]^2 \tag{11}$$

Equation 11 indicates that an integral of the pth eigenfunction f_p is evaluated from experimentally determined g_p. For convenience of this evaluation, we classify f_p in two categories: Two ends of a linear chain should move in an equivalent fashion, so that f_p should be either symmetrical ($f_p(n) = f_p(N\text{-}n)$) or antisymmetrical ($f_p(n) = -f_p(N\text{-}n)$) with respect to the chain center ($n=N/2$). The symmetrical f_p are classified as odd f_p (with $p = 1, 3, \ldots$), and the antisymmetrical f_p, as even f_p ($p = 2, 4, \ldots$). Then, as seen from eq 11, an integral of f_p defined by

$$F_p(n^*) = \frac{\sqrt{2}}{N}\int_0^{n^*} f_p(n)\, dn \ (=0 \text{ for } n^* = 0) \tag{12}$$

is evaluated as

$$F_p(N/2) - F_p(n^*) = \pm[g_p(n^*)/4\Delta\epsilon]^{1/2} \ (=0 \text{ for } n^* = N/2); \quad p = \text{odd} \tag{13a}$$

Table I. Characteristics of Dipole-Inverted PI Samples

code	$10^{-3}M^a$	M_w/M_n	$r_{UV}{}^b$	$r_M{}^c$	first precursor $10^{-3}M_1{}^a$	first precursor M_w/M_n	second precursor $10^{-3}M_2{}^a$	second precursor M_w/M_n
I-I 49-0[d]	48.8	1.05			48.8	1.05		
I-I 50-6	55.4	1.06	1.03	1.01	49.9	1.05	6.12	1.08
I-I 35-9	44.4	1.05	1.04	1.00	35.0	1.04	9.48	1.04
I-I 35-14	47.6	1.07	0.96	1.02	34.7	1.05	13.7	1.04
I-I 33-16	48.9	1.07	0.98	0.99	32.6	1.07	15.7	1.04
I-I 28-18	47.4	1.06	0.96	0.96	27.5	1.04	18.0	1.04
I-I 24-24[e]	47.7	1.06			23.9	1.05		

[a] Weight-average molecular weight. [b] $r_{UV} = (A_c + A_1 + A_2)/A_t$. [c] $r_M = (M_1 + M_2)/M$. [d] Regular PI without dipole inversion. [e] I-I 24-24 with symmetrically inverted dipoles was made in our previous work[10] *via* one-step coupling of precursor PI.

and

$$F_p(n^*) = \pm[g_p(n^*)/4\Delta\epsilon]^{1/2}\ (=0 \text{ for } n^* = 0); \quad p = \text{even} \tag{13b}$$

When $g_p(n^*)$ is obtained for the dipole-inverted PI chains with various n^* values = 0, n_1^*, n_2^*, ..., $N/2$ increasing in this order, we can choose either $+[g_p/4\Delta\epsilon]^{1/2}$ or $-[g_p/4\Delta\epsilon]^{1/2}$ for $n^* = 0$ in eq 13a and for $n^* = n_1^*$ in eq 13b, because $f_p(n)$ and $-f_p(n)$ are equivalent eigenfunctions and thus either $F_p(n^*)$ or $-F_p(n^*)$ can be used as the integral. For definiteness, we choose $+[g_p/4\Delta\epsilon]^{1/2}$ in this paper. With this constraint, a requirement of smooth and continuous n^* dependence of $F_p(n^*)$ unequivocally determines the signs of the terms $[g_p(n^*)/4\Delta\epsilon]^{1/2}$ in eq 13 for the other n^* values, if the intervals between the neighboring n^* values are sufficiently small. This was the case for the determination of $F_p(n^*)$ (p = 1–3) made in this paper for seven n^* values in a range $0 \le n^* \le N/2$ (cf. Table I). For $n^* > N/2$, eigenfunction symmetries lead to the relations $F_p(n^*) = -F_p(N\text{-}n^*) + 2F_p(N/2)$ for p = odd and $F_p(n^*) = F_p(N\text{-}n^*)$ for p = even. Thus, from g_p (p = 1–3) obtained for $0 \le n^* \le N/2$, we unequivocally evaluated $F_p(n^*)$ in an entire range $0 \le n^* \le N$ through eq 13.

Those $F_p(n^*)$ provide us information on detailed aspects of global chain motion. For example, for a vector connecting the n_1 and n_2th segments, $\mathbf{R}_{12}(t) = \int_{n_1}^{n_2}\mathbf{u}(n,t)\,dn$, an autocorrelation function is given by

$$\Phi_{12}(t) = \frac{\langle \mathbf{R}_{12}(t)\cdot\mathbf{R}_{12}(0)\rangle}{\langle \mathbf{R}_{12}{}^2\rangle} = \frac{N}{n_2\text{-}n_1}\sum_{p=1}^{N}[F_p(n_2) - F_p(n_1)]^2 \exp(-t/\tau_p) \tag{14}$$

This equation indicates that relaxation is faster for the portion of the chain that has smaller $[F_p(n_2) - F_p(n_1)]^2$ values for the low-order eigenmodes. Thus, we used the experimental F_p's and examined differences of the relaxation rates for various portions of the chain, as shown later in Figure 10. Furthermore, we may obtain a clue to specify the features of a time evolution equation for $C(n,t;m)$ and thus those of the global chain motion, if we know eigenvalues $1/\tau_p$ and eigenfunctions f_p (or F_p) up to sufficiently high mode number p. This possibility encourages the dielectric work on the dipole-inverted PI chains.

Here, we add a few comments on our final formulas (eqs 10, 12, and 13). These equations were derived for a dielectric response of a single chain and are best applied to *dilute* blends containing a small amount of dipole-inverted PI chains dissolved in dielectrically inert (non-type-A) matrices like polybutadiene. For monodisperse *bulk* systems of the PI chains examined in this paper, we need to consider, *in principle*, an orientation correlation for all chains in the system and modify the fundamental relation, eq 1, as[14]

$$\Phi(t) \propto \sum_i\sum_j \langle \Delta\mathbf{R}_i(t)\cdot\Delta\mathbf{R}_j(0)\rangle = \sum_i \langle \Delta\mathbf{R}_i(t)\cdot\Delta\mathbf{R}_i(0)\rangle + \sum_i\sum_{j\neq i} \langle \Delta\mathbf{R}_i(t)\cdot\Delta\mathbf{R}_j(0)\rangle \tag{1'}$$

Here, $\Delta\mathbf{R}_i$ is the difference vector (cf. Figure 1) of the ith chain in the system. However, the product $\Delta\mathbf{R}_i(t)\cdot\Delta\mathbf{R}_j(0)$ involved in the second term of eq 1′ would take positive and negative values with the same probability if a dipole–dipole interaction energy is much smaller than a thermal energy, as is the case for the PI chains having only small dipole moments. Then, eq 1′ can be reduced to eq 1, so that we may safely apply eqs 10, 12, and 13 to monodisperse bulk systems of the dipole-inverted PI chains. (This argument is in harmony with an experimental fact that the dielectric relaxation mode distribution is the same in monodisperse systems and in dilute blends for PI chains either with symmetrical inversion of dipoles or with no inversion.[14])

III. Experimental Section

III.1. Synthesis. A series of monodisperse *cis*-polyisoprene (PI) samples having almost the same M (≅48 × 10³) but differently located dipole-inversion points were prepared. A PI sample without dipole inversion (i.e., inversion at one chain end) was obtained *via* our laboratory routine of anionic polymerization in high vacuum using *sec*-butyllithium (s-BuLi) and heptatne (Hep) as the initiator and solvent. A PI sample with *symmetrically* inverted dipoles (i.e., inversion at the chain center) was previously made *via* one-step coupling of monodisperse PI anions with a prescribed amount (≅90% equimolar to the PI anions) of *p*-xylylene dichloride (XDC) and successive fractionation.[10] Five PI samples with *asymmetrically* inverted dipoles (i.e., inversion not at the chain center) were synthesized in this study by a *multistep* coupling method, as summarized in Scheme I. This method was originally developed for syntheses of block polymers, and the details were described elsewhere.[18]

As shown in Scheme I, the method splits the coupling of two living PI precursors of molecular weights M_1 and M_2 (made in Hep) into several steps. In the first step, to a vigorously stirred *dilute* Hep solution of the first PI precursor anions (with $M_1 >$ 24 × 10³) was added at −78 °C a *large* amount of XDC (≅30–40 times excess to the anions) diluted with tetrahydrofuran (THF). Immediately after the addition, single-chain termination was completed and the first precursors with chlorinated ends (PI-Cl) were obtained as a major product. When necessary, the living ends of the precursors were converted to diphenylethylene (DPE) anions through a reaction with ~2 times excess DPE just before the addition of XDC (case II of Scheme I). This end modification enabled us to reduce the amount of a minor product, dimers of the precursors formed by bimolecular termination.

In the second step, the first-step product was precipitated in pure acetone (a nonsolvent for PI) to largely reduce the amount of unreacted (excess) XDC left with the product. After removal of the supernatant containing excess XDC, the precipitated product was thoroughly dried and then redissolved in pure THF. The whole precipitation/redissolution procedure was repeated in *high vacuum* several times,[18] and the PI-Cl/THF solution containing only a small amount of residual XDC was recovered (cf. part b of Scheme I).

In the third step, the PI-Cl chains were allowed to couple with 2–3 times excess of the second precursor PI anions (with $M_2 < M_1$) at ≅ 30 °C for 2–3 days to yield dipole-inverted PI chains (cf. part c of Scheme I). (Dimers of the second precursors were also formed as a minor product due to residual XDC, but they were removed by later fractionation.) For convenience for later characterization, the living ends of the second precursors were converted to DPE anions when DPE was not used in the first step (case I of Scheme I), and vice versa (case II).

Scheme I. Synthesis of PI chains with Asymmetrically Inverted Dipoles *via* Multistep Coupling

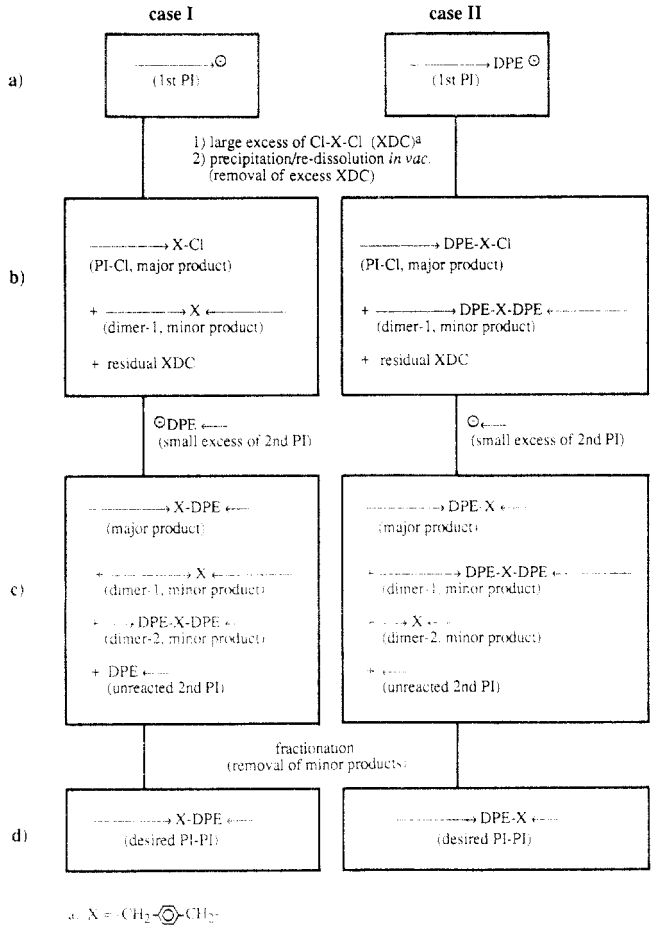

[a] X = $-CH_2-C_6H_4-CH_2-$

Finally, after fractionation of the third-step product from benzene/methanol solutions, we obtained dipole-inverted PI chains composed of two PI blocks of molecular weights M_1 and M_2 (cf. part d of Scheme I): The direction of the parallel dipoles is the same in each block but inverted at the junction between the two blocks.

III.2. Characterization. The products obtained at respective stages of the multistep coupling were characterized with a gel permeation chromatograph (GPC) having a combined refractive index (RI) and light scattering (LS) monitor (Tosoh, LS-8000) and an ultraviolet (UV) absorption monitor (Tosoh, UV-8011). The elution solvent was THF, and previously made and characterized monodisperse PI chains[10] were used as elution standards.

Through the multistep coupling, a UV-active coupler unit composed of *p*-xylylene and DPE groups was attached to each PI chain (cf. part d of Scheme I). This low-M unit had no detectable contribution to the RI and LS signals for the high-M PI chains made in this study. However, since the isoprene unit has very weak UV absorption (at $\lambda = 254$ nm), even one coupler unit per chain drastically increased the UV signal. Using this feature, we examined the coupler/isoprene composition at various stages of the multistep coupling through the UV signal. (Coupling of the PI-Cl chain and the second PI precursor with the DPE anion end induced a large change of the UV signal *even when the former was much longer than the latter.* Thus, for easy characterization of the final product, we used the end-modified second precursor in case I of Scheme I.)

As an example of the UV and RI signals of the products at various stages of the reaction, Figure 2 shows those for case II (cf. Scheme I) with $M_1 = 34.7 \times 10^3$ and $M_2 = 13.7 \times 10^3$. The signal sensitivities are the same for all GPC traces a–e, so that the changes of the coupler/isoprene composition during the reaction are seen in the figure as the differences of the UV/RI signal ratios for the traces. For the main peaks of traces a and b obtained before and after the reaction of the first PI precursor with DPE and XDC, we find that the RI signal is the same but

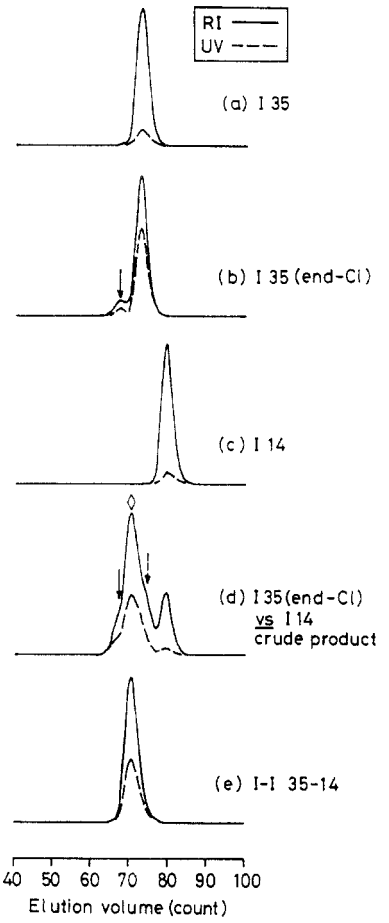

Figure 2. GPC traces for products obtained at various stages of synthesis of a dipole-inverted PI sample with $M_1 = 34.7 \times 10^3$ and $M_2 = 13.7 \times 10^3$. The RI and UV signal sensitivities are the same for all traces. The solid and dashed arrows for parts b and d indicate the dimers of the first and second precursors, respectively. These minor components were formed through a bimolecular termination of living precursor anions by *p*-xylylene dichloride. The diamond-shaped arrow for trace d indicates the location of a GPC trace for the desired dipole-inverted PI chain having $M = M_1 + M_2$.

the UV signal is much larger for the latter. Thus, the coupler units were successfully attached to the precursor ends to obtain the PI-Cl chains as the main product. (Although a small amount of the dimers is seen for trace b at a location corresponding to $2M_1$ (the solid arrow), they were removed by later fractionation.)

GPC trace b of the first-step product was not affected by the precipitation/redissolution procedure (cf. Scheme I) and changed to trace d after reaction with the second precursor PI anions (trace c). The UV/RI signal ratio for the main peak of trace d is certainly smaller than that for the main peak of trace b. In addition, we found that the former peak appeared at a location corresponding to $M = M_1 + M_2$ (shown with the diamond-shaped arrow). These results indicate a successful coupling of the two precursors. Finally, a small amount of undesired components, unreacted (excess) second precursors, their dimers (dashed arrow for trace d), and the dimers of the first precursors (solid arrow), was removed by fractionation to obtain the final product composed of two PI blocks and a coupler unit (trace e).

For the PI precursors and the dipole-inverted PI chains (final product), the weight-average molecular weights M_w and heterogeneity indices M_w/M_n were evaluated from the RI signals with an elution volume calibration (made for the standard PI's[10]). The M_w values were determined also from the LS signals, and good agreements were observed. The results of the characterization are summarized in Table I, where the sample code numbers indicate the molecular weights M_1 and M_2 of the two precursors in units of 1000. As seen there, the molecular weight M is nearly the same for all PI samples used in this study.

In addition to the RI and LS signals, the UV signals were analyzed to evaluate a quantity

$$r_{UV} = \frac{A_c + A_1 + A_2}{A_f} \quad (15)$$

Here, A_1 and A_2 are the *molar* UV absorption for the first and second PI blocks involved in the final product (cf. part d of Scheme I), respectively, and A_c and A_f are the molar absorption for the coupler unit and the final product, respectively. We should have $r_{UV} = 1$, if the final product contains only the desired PI chains with asymmetrically inverted dipoles. Thus, the quantity r_{UV} was used as a measure for the quality of that product.

A_1 and A_2 were evaluated from the UV data and molecular weights of the PI precursors recovered before the reaction with DPE and XDC (cf. Scheme I). Similarly, A_f were evaluated from the UV data and M for the final product. For evaluation of A_c for case I of Scheme I, we measured the molar UV absorption A_x for *p*-xylene and $A_{2\text{-DPE}}$ for the end-modified second precursor recovered after the reaction with DPE. The difference $\Delta A_2 = A_{2\text{-DPE}} - A_2$ represents the molar absorption of the DPE unit involved in that precursor, and A_c was evaluated as $\Delta A_2 + A_x$. For case II, we replaced the chlorine atom at the end of the first precursor (cf. part b of Scheme I) by an isoprene pentamer through an end-capping reaction with a large amount of living pentamer anions. 100% replacement was easily achieved within 1 h for this reaction involving oligoanions. From the molar UV absorption $A_{1\text{-c-p}}$ for the resulting end-capped precursor, A_c was evaluated as $A_{1\text{-c-p}} - A_1$.

The r_{UV} values calculated from the A values are summarized in Table I together with the other measure for the product quality, $r_M = (M_1 + M_2)/M$ with M_1, M_2, and M being the molecular weights of the two PI precursors and the final product, respectively. As seen there, both r_{UV} and r_M values are identical to unity within experimental uncertainties, indicating that the desired PI chains with asymmetrically inverted dipoles were successfully obtained.

III.3. Measurements. Dielectric loss factors ϵ'' were measured at $40 \le T$ (°C) ≤ 80 with capacitance bridges (GR 1615A, General Radio; Precision LCR-meter 4284A, Hewlett-Packard) on monodisperse bulk systems of the PI systems. The time–temperature superposition worked very well, and the ϵ'' data were reduced at $T_r = 40$ °C. The shift factors a_T for the dipole-inverted PI chains were identical to the previously reported a_T for regular PI chains without inversion,[9,10] suggesting that the small coupler units involved in the former did not affect the chain motion. (In the temperature range examined, the amount of the shift was less than 1 decade and ambiguities due to the shift were negligibly small.)

IV. Results

Dielectric Loss Curves. Figure 3 shows the frequency (ω) dependence of ϵ'' at 40 °C for the PI chains with various locations of the dipole-inversion points.[19] Those PI chains having $M \cong 10M_e$ ($M_e \cong 5000$ for bulk PI[1,2]) are rather heavily entangled in their monodisperse bulk systems. In Figure 3, respective ϵ'' curves are shifted vertically to avoid heavy overlapping of the data points. Details for differences of the curves can be more clearly examined in Figure 4, where the data points are not shown and no vertical shifts are made.

As seen in Table I, the molecular weights are close but not exactly the same for the PI chains examined. Correspondingly, the longest relaxation time τ_1 for the local correlation function (cf. eq 7) is slightly different for those PI chains. Throughout this section (including Figures 3 and 4), we use the I-I 24-24 sample ($M = 47.7 \times 10^3$) as a reference and shift the ϵ'' curve of each PI sample along the ω axis by a factor $a_M = (M/47.7 \times 10^3)^{3.5}$ to correct the difference of τ_1. ($\tau_1 \propto M^{3.5}$ for monodisperse chains.[10]) The log a_M values are summarized in Table II.

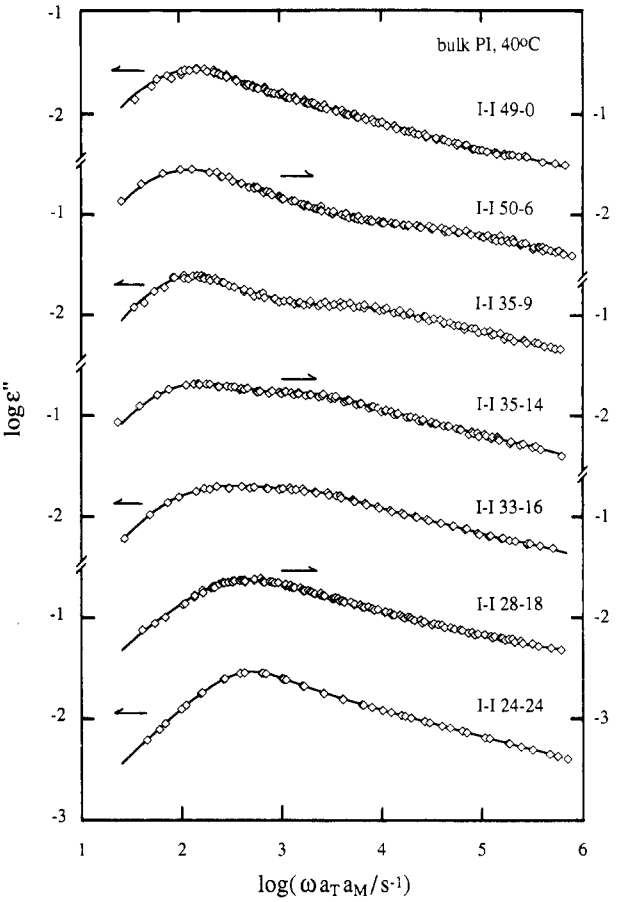

Figure 3. Frequency (ω) dependence of the dielectric loss factors ϵ'' at 40 °C for the dipole-inverted PI chains. Small differences of the longest relaxation times τ_1 of the PI chains are corrected by shifts of the ϵ'' curves along the ω axis by factors $a_M = (M/47.7 \times 10^3)^{3.5}$. (The I-I 24-24 chain with $M = 47.7 \times 10^3$ was used as a reference for this shift.) Respective curves are further shifted vertically to avoid heavy overlapping of the data points.

The small coupler units involved in the long PI chains should have no effect on the global motion. Thus, after the small correction for τ_1 (with $|\log a_M| \le 0.1$ except for I-I 50-6 with $\log a_M \cong 0.2$), we can consider the motion of the PI chains to be exactly the same. Nevertheless, large differences of the ϵ'' curves are observed in Figures 3 and 4, because of the dielectric labeling due to dipole inversion: As the dipole-inversion point moves from the chain end (I-I 49-0) to the center (I-I 24-24), the ϵ'' peak intensity decreases at $\log \omega \cong 2.1$ and increases at $\log \omega \cong 2.7$, and the shape of the ϵ'' curve first becomes broad and bimodal and then becomes narrow again. These changes correspond to changes of the dielectric relaxation mode distribution and provide us information for the chain motion through eqs 10, 12, and 13.

In Figure 5, the ϵ'' curve for I-I 49-0 (after correction for τ_1) is shifted along the ω axis by a factor $\Delta_M = 3.9$ and compared with the curve for I-I 24-24. The two curves are indistinguishable, meaning that the relaxation mode distribution is the same for the I-I 49-0 and 24-24 chains but the *dielectrically observed* relaxation time is 3.9 times shorter for the latter.[10,14] As seen from eq 13, only odd eigenmodes of the chain motion contribute to ϵ'' of the I-I 49-0 chain (with $n^* = 0$), while only even modes contribute to ϵ'' of the I-I 24-24 chain (with $n^* = N/2$). Thus, the sharp ϵ'' peaks for these PI chains correspond to the first and second modes with relaxation times τ_1 and τ_2 ($=\tau_1/$

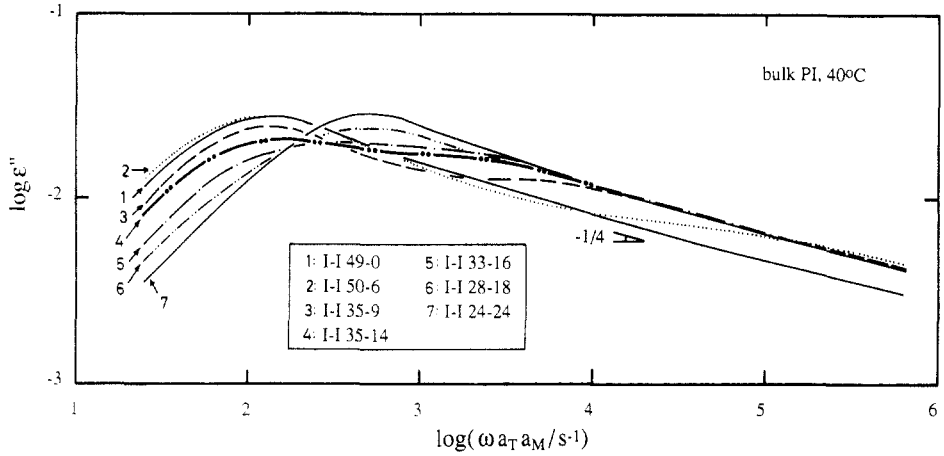

Figure 4. Comparison of the ϵ'' curves at 40 °C for the dipole-inverted PI chains. Only the curves smoothly connecting the data points are shown, and no vertical shifts are made. As done in Figure 3, horizontal shifts by factors $a_M = (M/47.7 \times 10^3)^{3.5}$ are made to correct small differences of τ_1.

Table II. Correction Factors for Small Differences of the Longest Relaxation Times τ_1 for the PI Samples

sample	log a_M[a]
I-I 49-0	0.035
I-I 50-6	0.227
I-I 35-9	−0.109
I-I 35-14	−0.003
I-I 33-16	0.038
I-I 28-18	−0.010
I-I 24-24	0

[a] $a_M = (M/M_{\text{I-I 24-24}})^{3.5}$.

3.9; cf. Figure 5). Specifically, the τ_1 and τ_2 values are evaluated from the peak frequencies as

$$\tau_1 = 8.13 \times 10^{-3}\ \text{s}, \qquad \tau_2 = 2.09 \times 10^{-3}\ \text{s} \qquad (16)$$

Eigenfunctions for $C(n,t;m)$. For evaluation of the integrals F_p of the eigenfunctions f_p, we have to decompose the ϵ'' curves of the dipole-inverted PI chains into contributions from the eigenmodes (cf. eqs 10, 12, and 13). Although we may do this with various methods, we here use a linear least-squares fitting method that enables us to analyze the ϵ'' data with the highest accuracy attainable.

F_1 and F_2 are evaluated from the ϵ'' data at low ω where the contribution from all higher pth modes with $p \geq 3$, $\sum_{p\geq 3} g_p(n^*)\, D_p(\omega)$ with $D_p(\omega) = \omega\tau_p/(1 + \omega^2\tau_p^2)$ (cf. eq 10), is practically identical to its low-ω asymptote,

$$G_3\omega = [\sum_{p\geq 3} g_p\tau_p]\omega \qquad (17)$$

At those low ω, eq 10 becomes a *linear* function of three variables g_1, g_2, and G_3,

$$\epsilon''(\omega;n^*) = g_1(n^*)\, D_1(\omega) + g_2(n^*)\, D_2(\omega) + G_3(n^*)\, \omega \qquad (18)$$

(Note that the locations of the two single-relaxation functions $D_1(\omega)$ and $D_2(\omega)$ are determined by τ_1 and τ_2 given in eq 16.) Thus, as explained in Appendix B, we made a standard linear least-squares fit with eq 18 to determine g_1, g_2, and G_3.

Figure 6 demonstrates the results of the mode decomposition. The unfilled symbols indicate the ϵ'' data, and the dash-dot and dashed curves, the contributions from the first and second modes g_1D_1 and g_2D_2, respectively. The contribution from all higher pth modes with $p \geq 3$, $\epsilon_{p\geq 3}'' = \epsilon'' - g_1D_1 - g_2D_2$, is shown with the filled symbols. We see that the prerequisite of the fit, $\epsilon_{p\geq 3}'' \propto \omega$, is well satisfied at low ω. This result indicates that the mode decomposition was well achieved and g_1 and g_2 were

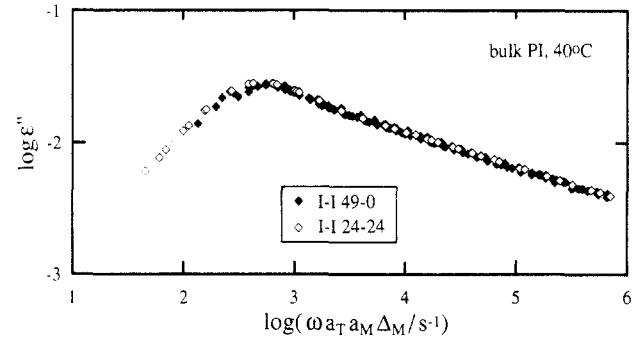

Figure 5. Comparison of the ϵ'' curves at 40 °C for the I-I 49-0 and I-I 24-24 chains. The curve for the former is shifted along the ω axis first by a factor $a_M = (48.8/47.7)^{3.5} = 1.083$ (a correction for the difference of τ_1) and further by a factor $\Delta_M = 3.9$.

determined with little ambiguities. From these g_1 and g_2 together with the total relaxation intensity $\Delta\epsilon$ (determined by integration of ϵ'' curves with respect to ln ω),[9,14] we evaluated F_1 and F_2 through eq 13. As explained earlier, a requirement of smooth and continuous n^* dependences of F_1 and F_2 was successfully used in this evaluation. (F_1 and F_2 monotonically increased with n^* for $0 \leq n^* \leq N/2$, as shown later in Figure 7.)

It is desirable to evaluate F_p also for higher modes ($p \geq 3$) from the linear least-squares fit for the ϵ'' data. We can accurately do this *if we know the τ_p values for $p \geq 3$ and those values are sufficiently separated.* The τ_p values would be experimentally determined from ϵ'' peak frequencies for a special sort of PI chains with *multiinversion* of dipoles, e.g., a PI chain with inversions at $n^* = N/3$ and $2N/3$ (that would exhibit a peak corresponding to τ_3). However, such PI chains are not yet available. Thus, we *tentatively* estimated $\tau_3 = 1.1 \times 10^{-3}$ s from the ϵ'' data of the I-I 49-0 chain with a method explained in Appendix C. As above, we used the $\tau_1 - \tau_3$ values and made a linear least-squares fit for the ϵ'' data at low ω with equation

$$\epsilon''(\omega;n^*) = g_1(n^*)\, D_1(\omega) + g_2(n^*)\, D_2(\omega) + g_3(n^*)\, D_3(\omega) + [\sum_{p\geq 4} g_p\tau_p]\omega \qquad (19)$$

From the resulting $g_1 - g_3$ values, we obtained F_3 together with the reevaluated F_1 and F_2. Although not shown here, a prerequisite of this fit, $\epsilon'' - g_1D_1 - g_2D_2 - g_3D_3 \propto \omega$, was satisified at low ω within a scatter similar to that seen in Figure 6. (For higher modes with $p \geq 4$, τ_p were not estimated with acceptably high accuracies and the mode decomposition was not made with good resolutions. Thus,

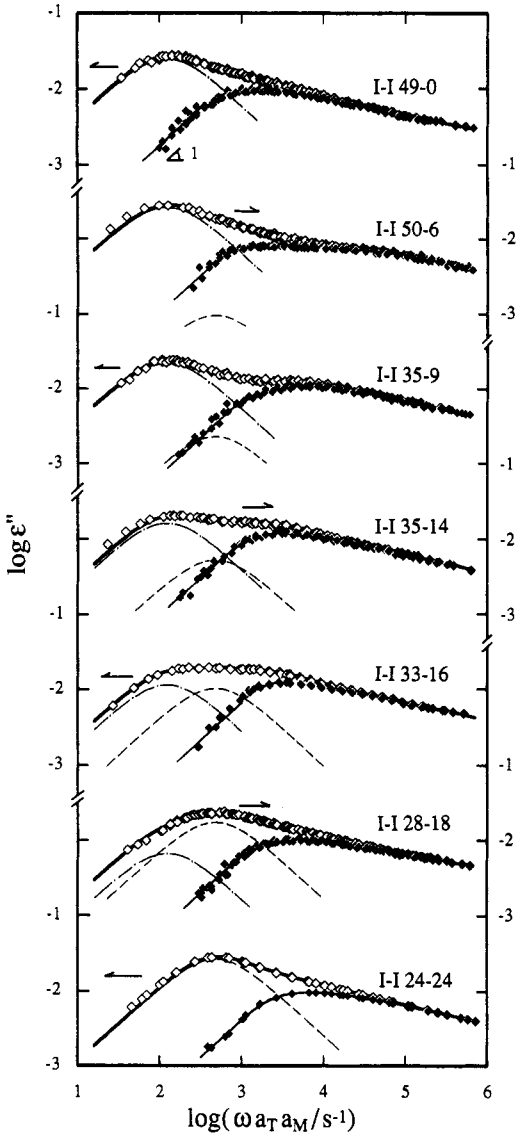

Figure 6. Results of the mode decomposition of the ϵ'' data (unfilled symbols) for the dipole-inverted PI chains at 40 °C. Linear least-squares fit with eq 18 was made for the decomposition. The dash-dot and dashed curves indicate the contributions from the first and second eigenmodes $g_1D_1(\omega)$ and $g_2D_2(\omega)$, respectively. ($D_p(\omega) = \omega\tau_p/(1+\omega^2\tau_p^2)$.) The contributions from all higher pth eigenmodes with $p \geq 3$, $\epsilon_{p\geq 3}''(\omega)$, are shown with the filled symbols. The thick solid curves indicate the recalculated $\epsilon'' = g_1D_1 + g_2D_2 + \epsilon_{p\geq 3}''$, with $\epsilon_{p\geq 3}''$ being evaluated for the thin solid curves that smoothly connect the filled symbols.

in this study we do not attempt to evaluate F_p for $p \geq 4$.)

Figure 7 shows the plots of $\Delta F_p(n^*) = F_p(n^*) - F_p(N/2)$ (p = 1–3) against n^*/N. (For convenience for later comparison, we have shown ΔF_p, not F_p themselves.) The unfilled and filled symbols indicate ΔF_p evaluated from the first and second least-squares fitting procedures using eqs 18 and 19, respectively. We may expect some ambiguities for the second procedure that involved the estimated τ_3 value. However, as seen in Figure 7, the two procedures gave almost identical ΔF_1 and ΔF_2. This result suggests an acceptably small ambiguity for the second procedure.

As explained later, some models have sinusoidal eigenfunctions, $f_p^\circ(n) = \sin(p\pi n/N)$.[6,14,21,22] The integrals of these f_p° (normalized according to eq 9) are given by

$$\Delta F_p^\circ(n^*) = \frac{\sqrt{2}}{p\pi}\left[\cos\frac{p\pi}{2} - \cos\frac{p\pi n^*}{N}\right] \qquad (20)$$

These ΔF_p° are indicated with the dashed curves in Figure 7. As seen there, ΔF_p° are fairly close to the experimental

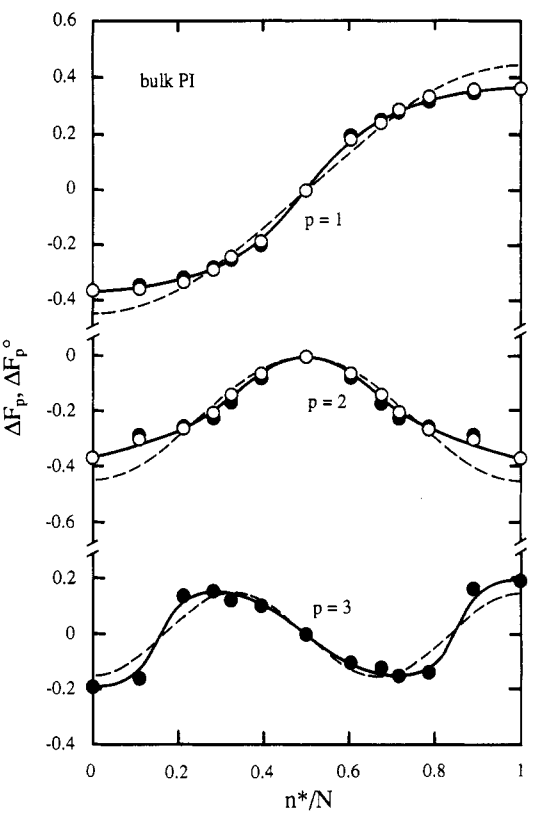

Figure 7. n^* dependence of the integrals of low-order eigenfunctions for the PI chains, $\Delta F_p(n^*) = -(\sqrt{2}/N)\int_n^{N/2} f_p(n)\,dn$ (= $F_p(n^*) - F_p(N/2)$; cf. eq 12). The unfilled and filled symbols indicate the experimental ΔF_p obtained from the linear least-squares fits for the ϵ'' data with eqs 18 and 19, respectively. The dashed curves indicate $\Delta F_p^\circ(n^*) = [2^{1/2}/p\pi][\cos(p\pi/2) - \cos(p\pi n^*/N)]$ predicted from the CDCR and reptation models. Note that $\Delta F_p(n^*)$ and $\Delta F_p^\circ(n^*)$ are normalized according to eq 9, so that their differences at $n^* = 0$, N suggest nonsinusoidal n dependences for the eigenfunctions $f_p(n) = [N/\sqrt{2}][d\Delta F_p(n)/dn]$ of actual PI chains.

ΔF_p for $n^* \cong N/2$ but systematically deviate from ΔF_p as n^* approaches 0 or N. The differences between ΔF_p and ΔF_p° seen for $n^* = 0$ and N are larger than the ambiguities in the evaluation of ΔF_p. Because the eigenfunctions f_p and f_p° and thus their integrals ΔF_p and ΔF_p° are normalized (cf. eq 9), those differences suggest some differences of the n^* dependences of f_p and f_p°. For a critical examination, we magnified ΔF_p° by adequate factors z_p (=0.79, 0.82, and 1.32 for p = 1–3) so that $z_p\Delta F_p^\circ$ coincided with ΔF_p at $n^* = 0$ and N, and compared $z_p\Delta F_p^\circ$ (dashed curves) with ΔF_p (symbols) in Figure 8. This comparison most clearly demonstrates the *nonsinusoidal* n dependences of the experimental $\Delta F_p(n)$ and $f_p(n) = [N/\sqrt{2}][d\Delta F_p(n)/dn]$, although deviations from sinusoidal dependences are not very large.

V. Discussion

For relaxation processes in entangled blends as well as monodisperse systems with intermediate M ($\leq 20M_e$), the importance of the constraint release (CR) mechanism[20–22] has been experimentally established.[3,14,15,23] Thus, we compare the ϵ'' curves of the dipole-inverted PI chains with predictions of a configuration-dependent constraint release (CDCR) model.[14,15,22,23] This model assumes a Rouse-type CR[20,21] and allows it to compete with reptation[6,21] that is taking place simultaneously. Among various models so far proposed, the CDCR model appears to best describe this competition formulated for various kinds of local relaxation functions.[14,15,22,23]

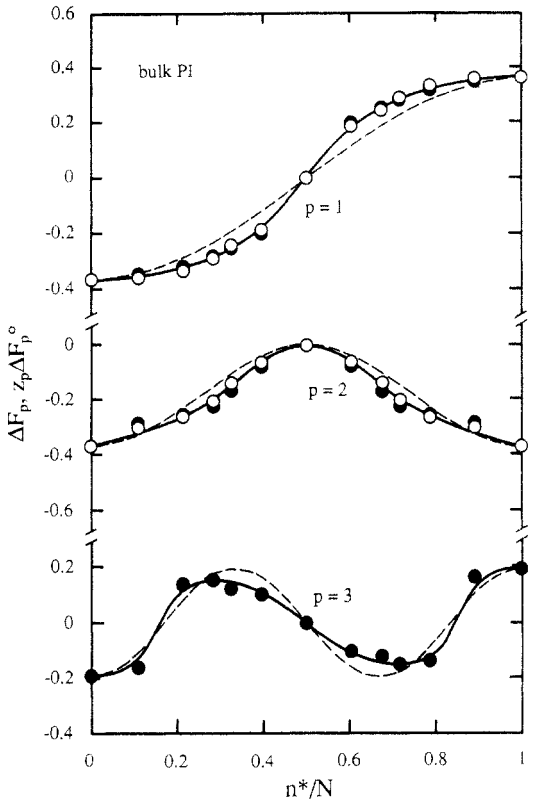

Figure 8. Critical comparison of $\Delta F_p^\circ(n^*)$ predicted from the CDCR and reptation models (dashed curves) with the experimental $\Delta F_p(n^*)$ (symbols). The former are magnified by adequate factors z_p (=0.79, 0.82, and 1.32 for p = 1–3) so that $z_p\Delta F_p^\circ$ coincide with ΔF_p at n^* = 0 and N.

For the local correlation function $C(n,t;m)$ of monodisperse PI chains composed of N entanglement segments, the CDCR model leads to a time evolution equation[14,15]

$$\frac{\partial}{\partial t}C(n,t;m) = \frac{1}{\tau_1^\circ}[N/\pi]^2\frac{\partial^2}{\partial n^2}C(n,t;m) \qquad (21)$$

Here, $\tau_1^\circ = [\tau_{rep}^{-1} + \tau_{CR}^{-1}]^{-1}$, with τ_{rep} ($\propto N^3$) and τ_{CR} ($\propto N^5$) being the pure reptation and CR times, respectively. (This τ_1° is roughly proportional to $N^{3.4}$ for intermediately large N.) With the boundary and normalization conditions, eqs 8 and 9, the pth eigenfunctions and eigenvalues associated with eq 21 are given by

$$f_p^\circ(n) = \sin\frac{p\pi n}{N}, \quad 1/\tau_p^\circ = p^2/\tau_1^\circ \qquad (22)$$

Using these $f_p^\circ(n)$ and τ_p°, we can calculate $\epsilon''(\omega;n^*)$ for the PI chain with dipole inversion at the n^*th segment. Note that the time evolution equation is given by eq 21 also for the *pure* reptation model.[6,21] Thus, despite the difference of τ_1° for the CDCR and reptation models ($\tau_1^\circ = \tau_{rep} \propto N^3$ for the latter), the results explained below are applicable also to the reptation model.

From eqs 10, 12, 13, and 22, we first find a relation

$$\epsilon''(\omega;N/2) = \frac{8\Delta\epsilon}{\pi^2}\sum_{p=odd}\frac{1}{p^2}\frac{\omega\tau_1^\circ/4p^2}{1+(\omega\tau_1^\circ/4p^2)^2} = \epsilon''(\omega/4;0) \qquad (23)$$

Namely, the model predicts that the $\epsilon''(\omega;0)$ curve for I-I 49-0 is superposed on the $\epsilon''(\omega;N/2)$ curve for I-I 24-24 if the former is shifted along the ω axis by a factor Δ_M = 4. This is in close agreement with the experimental result shown in Figure 5. For further examination of the model, Figure 9 shows the ϵ'' curves calculated for a series of PI chains having the same N but different n^*. The n^*/N ratios are the same as the M_2/M ratios for the actual PI samples (cf. Table I). The values of τ_1 and $\Delta\epsilon$ (dielectric relaxation intensity) were adequately chosen in the calculation so that the location and peak height of the ϵ'' curve calculated for the I-I 49-0 chain are the same as those observed experimentally (cf. Figure 4). For simplicity, small molecular weight distributions (MWD) of the PI chains were not considered in the calculation.

Comparing Figures 4 and 9, we note that general features of the dipole-inverted PI chains are reasonably well described by the CRCR model. In particular, for PI chains with n^*/N = 0 and $^1/_2$, our previous work indicated that the location and shape of the ϵ'' curves at low ω were semiquantitatively described by the CDCR model considering a small MWD.[14,15] However, a close inspection of Figures 4 and 9 reveals that the agreements become poorer for intermediate n^*/N even at low ω. (For example, compare the observed and calculated curves for the I-I 35-14 sample.) In addition, the calculated ϵ'' depends on ω too strongly at high ω ($\epsilon'' \propto \omega^{-1/2}$ irrespective of n^*), as already found for the cases of n^*/N = 0 and $^1/_2$.[10,14,15] These disagreements are not completely removed even if a small MWD is considered in the calculation. Thus, the CDCR model of the present form (eq 21) is valid only at low ω in a semiquantitative way. In other words, the Rouse-type CR and reptation processes considered in the model are not enough to describe the global motion of the entangled chains.

The experimentally observed τ_p (p = 1–3) are approximately proportional to p^{-2}, and the differences from the calculated τ_p° (eq 22) are rather small. However, as found in Figures 7 and 8, the observed and calculated eigenfunctions $f_p(n)$ and $f_p^\circ(n)$ certainly have different n dependences. This difference mainly caused the above disagreements of the ϵ'' curves at low ω. We can examine even more clearly an importance of the n dependence of $f_p(n)$ in the relaxation behavior through an autocorrelation function for a portion of the chain (*subchain*) between the n_1 and n_2th segments, $\Phi_{12}(t) = \langle \mathbf{R}_{12}(t)\cdot\mathbf{R}_{12}(0)\rangle/\langle \mathbf{R}_{12}^2\rangle$. ($\mathbf{R}_{12}$ is a vector connecting the n_1 and n_2th segments.) As seen from eq 14, the relaxation is faster for a subchain that has smaller $[F_p(n_2) - F_p(n_1)]^2$ values for the low-order eigenmodes (or equivalently, smaller $[f_p(n)]^2$ values in an interval $n_1 < n < n_2$).

For three subchains having almost the same length ($n_2 - n_1 \cong 0.11N$) but different locations, we used the experimental ΔF_p and τ_p (p = 1–3) to calculate Φ_{12} for $t > \tau_3$. (Higher order pth eigenmodes with $p \geq 4$ have negligible contributions to Φ_{12} at those long time scales.) Figure 10 shows those Φ_{12} plotted against t/τ_1 (symbols). For comparison, Φ_{12}° of the subchains calculated from the CDCR and reptation models are indicated with the solid curves. Both Φ_{12} and Φ_{12}° exhibit qualitatively the same feature, slower decay at the chain center than at the ends. In particular, for the subchain near the chain center, Φ_{12} is fairly close to Φ_{12}°. However, we also note for the subchain near the chain end that Φ_{12} decays much more rapidly than Φ_{12}°. Thus, actual PI chains may have an extra relaxation mechanism (other than reptation and Rouse-type CR) that has a significant effect at the chain ends but not so much at the center.

The CDCR model does not consider such an extra mechanism, and it treats the chain ends only as a memory-vanishing boundary to predict the sinusoidal f_p° (cf. eqs 21 and 22). Qualitatively, f_p° is distorted toward the experimental f_p when the extra mechanism is incorporated in the model and its effect is represented as a relaxation source $U(n)$ added in eq 21: $U(n)$ should be large for $n \cong 0$, N to have large effects at the chain ends. The

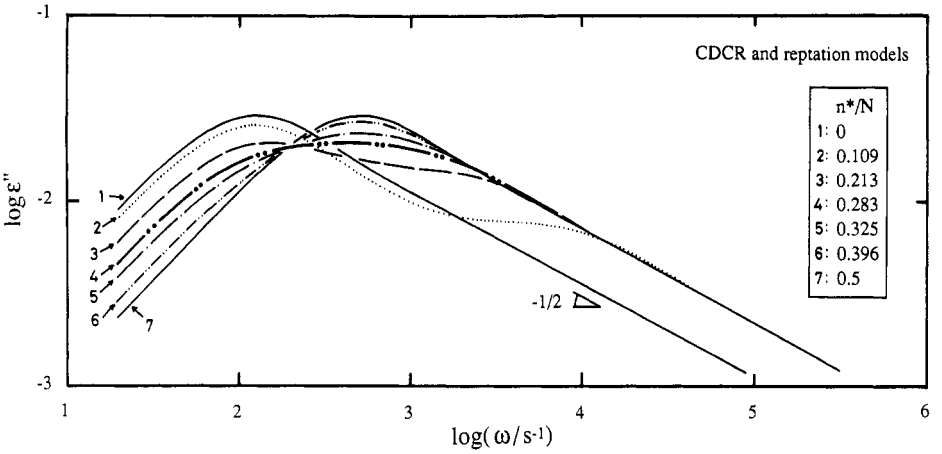

Figure 9. ϵ'' curves for the dipole-inverted PI chains calculated from the CDCR and reptation models. The longest relaxation time τ_1 and relaxation intensity $\Delta\epsilon$ were adequately chosen in the calculation so that the height and location of the ϵ'' peak were the same for the calculated and observed ϵ'' curves for the I-I 49-0 chain (cf. Figure 4). The numbers attached to the curves correspond to those in Figure 4.

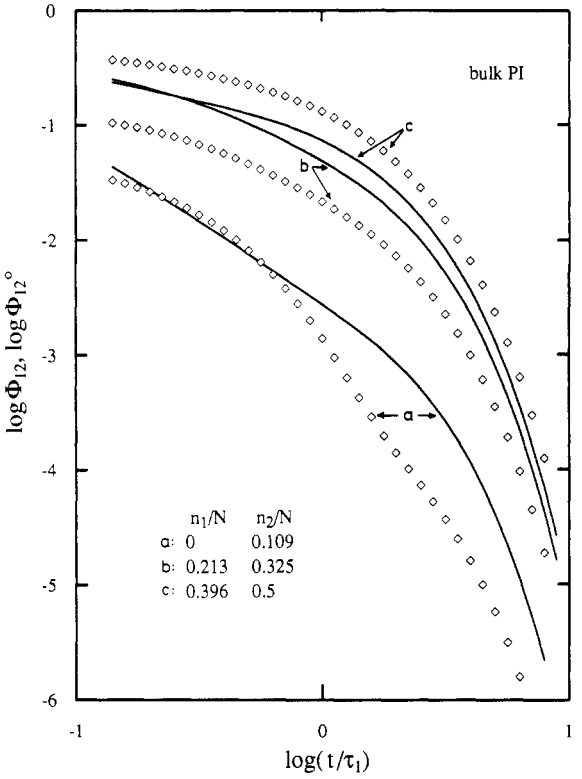

Figure 10. Decay of autocorrelation functions, $\Phi_{12}(t) = \langle \mathbf{R}_{12}(t)\cdot\mathbf{R}_{12}(0)\rangle/\langle \mathbf{R}_{12}^2\rangle$, for the three subchains as indicated. These subchains have almost the same length n_2-n_1 but different locations $(n_1/N, n_2/N)$. The symbols indicate $\Phi_{12}(t)$ evaluated from $\Delta F_p(n^*)$ and τ_p (p = 1–3) for the PI chains, and the solid curves, predictions of the CDCR and reptation models.

eigenfunction equation is formally identical to the Schrödinger equation with a potential term $U(n)$,

$$\frac{1}{\tau_p} f_p(n) = -\frac{1}{\tau_1^\circ}[N/\pi]^2 \frac{d^2}{dn^2} f_p(n) + U(n)\, f_p(n) \quad (24)$$

and $[f_p(n)]^2$ is analogous to the probability density. Thus, f_p and f_p° ($=f_p$ for $U=0$) normalized by eq 9 would satisfy a relation, $|f_p(n)| < |f_p^\circ(n)|$ for $n^* \cong 0, N$, as noted in Figure 7 for $f_p(n) = [N/\sqrt{2}][d\Delta F_p(n)/dn]$ (in particular for those with p = 1 and 2). (A similar argument may be made also for $U(n)$ that works as a differential operator.)

The above argument suggests a possible direction for refinement of the CDCR model or even gives a clue for the formulation of an entirely new model. However, a molecular motion inducing the extra relaxation is not yet specified. Analyses for the experimental $f_p(n)$ and τ_p up to sufficiently large p may provide a clue to find the features of this motion. On the other hand, some candidates for that motion may be found in molecular models: For example, contour length fluctuation[6] may induce a significant relaxation at the chain ends. However, to our knowledge the eigenfunctions for this mechanism have not been explicitly obtained, and a critical comparison with f_p cannot be made at this moment. These problems require further work both experimentally and theoretically.

VI. Concluding Remarks

The dielectric study on the dipole-inverted PI chains has provided us entirely new information for some details of eigenfunctions $f_p(n)$ for the local correlation functions $C(n,t;m)$. Differing from the prediction of the CDCR (as well as reptation) model, the experimentally obtained $f_p(n)$ (p = 1–3) have nonsinusoidal n dependence. This dependence appears to be related to an extra relaxation mechanism (other than reptation and Rouse-type CR) that has a significant effect at the chain ends.

In addition to the new information, the importance of the present work is also found in its idea of the experimental determination of the eigenfunctions. This idea is not limited to dielectric relaxation but applies to any relaxation process, for example, to a dichroism relaxation process of partly deuterated chains that can provide information for a segmental orientation tensor $\mathbf{S}(n,t) = \langle \mathbf{u}(n,t)\,\mathbf{u}(n,t)\rangle$. Thus, the idea of the present work would be useful for combining the detailed information for various kinds of local relaxation functions (e.g., $C(n,t;m)$ and $\mathbf{S}(n,t)$) to constract a unified molecular picture, as is extremely important for the deeper understanding of polymer dynamics.

Appendix A. Eigenfunction Expansion of $C(n,t;m)$

As a quantity that describes the fundamental features of the dielectric relaxation of type-A PI chains, a local correlation function is defined by

$$C(n,t;m) = (1/a^2)\langle \mathbf{u}(n,t)\cdot\mathbf{u}(m,0)\rangle \quad (A1)$$

with $\mathbf{u}(n,t)$ being a bond vector for the nth segment at time t and $a^2 = \langle \mathbf{u}^2\rangle$. At short time scales, the relaxation spectrum might be continuous and an eigenfunction expansion of $C(n,t;m)$ might contain some ambiguities. However, this is not the case at long time scales where the PI chains actually exhibit a terminal dielectric relaxation

that is decomposed into well-defined modes. These dielectric modes correspond to eigenmodes of $C(n,t;m)$, justifying the eigenfunction expansion at long time scales. For those cases, a time evolution of $C(n,t;m)$ should be generally described by an equation of a factorized form

$$\frac{\partial}{\partial t} C(n,t;m) = L(n)\, C(n,t;m) \qquad \text{(A2)}$$

where $L(n)$ represents an operator with respect to n. (Note in eq A1 that $\mathbf{u}(m,0)$ does not change with time; thereby no operation with respect to m is involved in eq A2.) Details of the global chain motion can be found from a functional form of the operator $L(n)$ or, equivalently, from the form of the eigenfunctions $h_p(n)$ (p = 1, 2, ...) associated with $L(n)$. This indicates the importance of the dielectric work on the dipole-inverted PI chains that determines $h_p(n)$.

Using $h_p(n)$ and corresponding eigenvalues $1/\tau_p$ that are determined by

$$L(n)\, h_p(n) = -(1/\tau_p)\, h_p(n) \quad (p = 1, 2, ..., N) \qquad \text{(A3)}$$

we can generally solve eq A2 as

$$C(n,t;m) = \frac{2}{N}\sum_{p=1}^{N} h_p(n)\, A_p(m)\, \exp(-t/\tau_p) \quad (t > 0) \qquad \text{(A4)}$$

Here, the factor $(2/N)A_p(m)$ represents the amplitude factor for the pth eigenfunction at $t = 0$. At equilibrium, an origin of time ($t = 0$) can be arbitrarily chosen and an orientation correlation of the bond vectors should be symmetrical with respect to time. This argument leads to a relation

$$\langle \mathbf{u}(n,t)\cdot\mathbf{u}(m,0)\rangle = \langle \mathbf{u}(n,0)\cdot\mathbf{u}(m,-t)\rangle = \langle \mathbf{u}(n,0)\cdot\mathbf{u}(m,t)\rangle \quad \text{for any } t, n, m \qquad \text{(A5)}$$

From eqs A1, A4, and A5, we find

$$A_p(m)\, h_p(n) = A_p(n)\, h_p(m) \quad \text{for any } n, m \qquad \text{(A6)}$$

and thus

$$A_p(n) = \alpha_p h_p(n) \qquad \text{(A7)}$$

Here, α_p is a numerical constant. Using normalized eigenfunctions $f_p(n) = \alpha_p^{1/2} h_p(n)$ in eqs A4 and A7, we finally find an expression for $C(n,t;m)$ on the basis of the eigenfunction expansion,

$$C(n,t;m) = \frac{2}{N}\sum_{p=1}^{N} f_p(n)\, f_p(m)\, \exp(-t/\tau_p) \quad (t > 0) \qquad \text{(A8)}$$

Appendix B. Determination of g_1 and g_2

At ω below a characteristic ω_c, the contribution to ϵ'' form all higher pth modes with $p \geq 3$, $\epsilon_{p\geq 3}''$, is practically identical to its low-ω asymptote, $G_3\omega = [\sum_{p\geq 3} g_p\tau_p]\omega$. Then, eq 10 becomes

$$\epsilon''(\omega;n^*) = g_1(n^*)\, D_1(\omega) + g_2(n^*)\, D_2(\omega) + G_3(n^*)\, \omega \qquad \text{(B1)}$$

with $D_k(\omega) = \omega\tau_k/(1 + \omega^2\tau_k^2)$ being a single-relaxation function for the kth mode. Using eq B1, we made a standard linear least-squares fit: Minimizing a sum $\sum[\epsilon'' - g_1D_1 - g_2D_2 - G_3\omega]^2/\epsilon''^2$ taken in the range of $\omega < \omega_c$, we obtained a set of linear equations that determined g_1, g_2, and G_3.

For the best fit to be made, the upper limit of the fitting range, ω_c, should be small enough so that eq B1 is valid. At the same time, ω_c should be large enough so that we can involve enough data points in the fit. Thus, we varied ω_c around its first estimate $1/\tau_2$ (=478 s^{-1}; cf. eq 16) and examined a quality of the fit. For respective PI samples, we found a range of the acceptable ω_c values: In that range, a mean-square deviation of the fit, δ, was minimized and the g_1, g_2, and G_3 values were insensitive to the choice of ω_c. The smallest value of the acceptable ω_c was used to finally determine the g_1, g_2, and G_3 values. That ω_c value was $\cong 0.5/\tau_2$ for the I-I 49-0 chain ($n^* = 0$), $\cong 2/\tau_2$ for the I-I 24-24 chain ($n^* = N/2$), and between $0.5/\tau_2$ and $1/\tau_2$ for the other PI chains. With the g_1 and g_2 values determined for these ω_c, a prerequisite of the fit, $\epsilon'' - g_1D_1 - g_2D_2 \propto \omega$, was well satisfied at low ω, for some cases even at ω somewhat higher than ω_c (cf. Figure 6). This result suggests that the best fit was made.

Note here that the optimum value of ω_c is related to the relaxation time τ_3 (=1.1 × 10^{-3} s for the best estimate; cf. Appendix C) and intensity g_3 of the third eigenmode. For large g_3, $\epsilon_{p\geq 3}''$ at $\omega < \omega_c$ is dominated by the contribution from the third mode $g_3D_3(\omega)$. Then, ω_c should be sufficiently smaller than $1/\tau_3$ for a good fit with small δ to be made. This was the case for the I-I 49-0 chains: For $\omega_c \cong 0.5/\tau_2$ used in the fit, $D_3(\omega)$ at $\omega < \omega_c$ agrees with its low-ω asymptote $\omega\tau_3$ within a few percent. On the other hand, for smaller g_3, the third mode contribution becomes less significant and ω_c can become larger, as were the cases for the other PI's. In particular, for the I-I 24-24 chains having $g_3 = 0$, we had $\omega_c \cong 2/\tau_2$ and still found the prerequisite, $\epsilon'' - g_2D_2 \propto \omega$, to be well satisfied up to $\omega \cong 1.3\omega_c$ (cf. Figure 6).

Appendix C. Estimation of τ_3 for the Third Eigenmode

For the I-I 49-0 chain without dipole inversion, only odd eigenmodes contribute to ϵ''. Thus, at low ω where the contribution from all higher pth modes with $p \geq 5$ is practically identical to its low-ω asymptote, $G_5\omega = [\sum_{p\geq 5} g_p\tau_p]\omega$, we may rewrite eq 10 as

$$\epsilon'' = g_1D_1(\omega) + g_3D_3(\omega) + G_5\omega \qquad \text{(C1)}$$

For convenience for the estimation of τ_3, this equation is further modified as

$$\delta'' = \omega^3[\epsilon'' - g_1D_1(\omega) - G_3\omega]^{-1} = -X - \omega^2 Y \qquad \text{(C2)}$$

with

$$D_1(\omega) = \frac{\omega\tau_1}{1 + \omega^2\tau_1^2} \qquad \text{(C3)}$$

and

$$G_3 = \sum_{p\geq 3} g_p\tau_p, \qquad X = \frac{1}{g_3\tau_3^3}, \qquad Y = \frac{1}{g_3\tau_3} \qquad \text{(C4)}$$

Since τ_1 was experimentally determined (eq 16) and g_1 and G_3 were evaluated from the least-squares fit with eq 18 (cf. Figure 6), we made a standard linear least-squares fit for the quantities δ'' calculated from the ϵ'' data: Minimizing a sum $\sum[\delta'' + X + \omega^2 Y]^2/\delta''^2$ taken for the data in a given range of ω, we obtained a set of linear equations for X and Y that determined $\tau_3 = (Y/X)^{1/2}$.

Equation C1 should be valid in a ω range with its upper limit ω_c' being located in the vicinity of $1/\tau_3$. Thus, for the fit, we first need to know an approximate value for τ_3. For this purpose, we used $\tau_3^\circ = \tau_1/9$ (predicted from the CDCR and reptation models) as a first estimate. As in Appendix B, we varied ω_c' around $1/\tau_3^\circ$, examined a mean-square deviation of the fit, and obtained τ_3 = 1.1 × 10^{-3} s as the best estimate.

References and Notes

(1) Ferry, J. D. *Viscoelastic Properties of Polymers*, 3rd ed.; Wiley: New York, 1980.
(2) Graessley, W. W. *Adv. Polym. Sci.* **1974**, *16*, 38.
(3) Green, P. F.; Mills, P. J.; Palmstrøm, C. J.; Mayer, J. W.; Kramer, E. J. *Phys. Rev. Lett.* **1984**, *53*, 2145. Green, P. F.; Kramer, E. J. *Macromolecules* **1986**, *19*, 1108.
(4) (a) Jarry, J. P.; Monnerie, L. *Macromolecules* **1979**, *12*, 316. (b) Tassin, J. F.; Monnerie, L.; Fetters, L. J. *Macromolecules* **1988**, *21*, 2404. (c) Lantman, C. W.; Tassin, J. F.; Monnerie, L.; Fetters, L. J.; Helfand, E.; Pearson, D. *Macromolecules* **1989**, *22*, 1184. (d) Tassin, J. F.; Baschwitz, A.; Moise, J. Y.; Monnerie, L. *Macromolecules* **1990**, *23*, 1879.
(5) (a) Kornfield, J.; Fuller, G.; Pearson, D. *Macromolecules* **1989**, *22*, 1334. (b) Ylitalo, C. M.; Fuller, G.; Abetz, V.; Stadler, R.; Pearson, D. *Rheol. Acta* **1990**, *29*, 543. (c) Ylitalo, C. M.; Kornfield, J.; Fuller, G.; Pearson, D. *Macromolecules* **1991**, *24*, 749. (d) Kornfield, J.; Fuller, G.; Pearson, D. *Macromolecules* **1992**, *25*, 5429.
(6) Doi, M.; Edwards, S. F. *The Theory of Polymer Dynamics*; Clarendon: Oxford, U.K., 1986.
(7) Stockmayer, W. H. *Pure Appl. Chem.* **1967**, *15*, 539.
(8) (a) Baur, M. E.; Stockmayer, W. H. *J. Chem. Phys.* **1965**, *43*, 4319. (b) Stockmayer, W. H.; Burke, J. J. *Macromolecules* **1969**, *2*, 647.
(9) Imanishi, Y.; Adachi, K.; Kotaka, T. *J. Chem. Phys.* **1988**, *89*, 7585; see the references therein for the earlier work (mostly for broad MWD PI).
(10) Yoshida, H.; Watanabe, H.; Adachi, K.; Kotaka, T. *Macromolecules* **1991**, *24*, 2981.
(11) Adachi, K.; Nishi, I.; Doi, H.; Kotaka, T. *Macromolecules* **1991**, *24*, 5843.
(12) Boese, D.; Kremer, F.; Fetters, L. J. *Macromolecules* **1990**, *23*, 829; **1990**, *23*, 1826.
(13) Patel, S. S.; Takahashi, K. M. *Macromolecules* **1992**, *25*, 4382.
(14) (a) Watanabe, H.; Yamazaki, M.; Yoshida, H.; Adachi, K.; Kotaka, T. *Macromolecules* **1991**, *24*, 5365. (b) Watanabe, H.; Yamazaki, M.; Yoshida, H.; Kotaka, T. *Macromolecules* **1991**, *24*, 5372.
(15) Watanabe, H.; Kotaka, T. *Chemtracts: Macromol. Chem.* **1991**, *2*, 139.
(16) Cole, R. H. *J. Chem. Phys.* **1965**, *42*, 637.
(17) For integer n and m, δ_{nm} (eq 5) is identical to the Kronecker delta.
(18) Watanabe, H.; Shimura, T.; Kotaka, T.; Tirrell, M. *Macromolecules*, in press.
(19) PI chains exhibit dielectric relaxations due to both type-A and type-B dipoles that are parallel and perpendicular to the chain contour, respectively. However, the relaxation due to type-B dipoles takes place at high ω and its contribution to the ϵ'' curves is extremely small in the ω range examined in this study. This was confirmed from the fact that for high-M ($\geq 20 \times 10^3$) PI chains (without dipole inversion) the ϵ'' curves in that ω range have a universal mode distribution determined only by the global chain motion.
(20) Klein, J. *Macromolecules* **1978**, *11*, 852.
(21) Graessley, W. W. *Adv. Polym. Sci.* **1982**, *47*, 67.
(22) Watanabe, H.; Tirrell, M. *Macromolecules* **1989**, *22*, 927.
(23) Watanabe, H.; Yamazaki, M.; Yoshida, H.; Kotaka, T. *Macromolecules* **1991**, *24*, 5573.